W-Band *E*-Plane Waveguide Bandpass Filter Based on Meander Ring Resonator

Kai-Da Xu, *Senior Member, IEEE*, Shengpei Xia, Ying-Jiang Guo, *Member, IEEE*, Jianlei Cui, Anxue Zhang, *Member, IEEE*, and Qiang Chen, *Senior Member, IEEE*

***Abstract*— A *W*-band *E*-plane waveguide bandpass filter (BPF) is proposed using an embedded substrate with two metal strips and a meander ring resonator. The center frequency, bandwidth, and skirt selectivity of the proposed BPF can be easily adjusted. A simplified *LC* equivalent circuit is given to understand the operational mechanism of the BPF structure and investigate the distributions of the transmission zeros and poles. To validate the idea and show the performance of the designed *W*-band BPF, a prototype example is manufactured and measured. The measurement results show that the waveguide BPF has a center frequency at 91.3 GHz with a bandwidth from 88.9 to 93.7 GHz, and the minimum insertion loss within the passband is 1.6 dB.**

***Index Terms*— Bandpass filter (BPF), meander ring resonators (MRRs), waveguide filter, *W*-band.**

I. Introduction

With the advent of 5G and beyond communications, the design of millimeter-wave bandpass filters (BPFs) has attracted an increasing number of attention by the researchers. Various design methods and techniques have been proposed in order to obtain high-frequency selectivity, low insertion loss (IL) in the passband, and high rejection level at the stopband. In [1], a micromachining technique using the thick SU-8 photoresist was presented to construct a *W*-band BPF with a pseudo-elliptical response. In [2], a fifth-order *W*-band waveguide BPF centered at 90 GHz with a Chebyshev response was proposed and fabricated by microlaser sintering process. Also, numerous planar millimeter-wave BPFs using microstrip gap waveguide [3] and single- or multilayer substrate integrated waveguide (SIW) structures [4]–[8] have been explored recently. Moreover, some BPF works were designed in standard semiconductor technologies, such as GaAs [9], [10], SiGe [11], [12], and so on.

Compared with the planar filters, waveguide filters have the advantages of low loss and high power capacity although large sizes are occupied. In some specific applications using higher operating frequencies, waveguide filters are preferred as the first choice [13], [14]. In the early stage, the *E*-plane metal septum was embedded in the standard rectangular waveguide to construct a waveguide BPF for ease of fabrication [15]. However, to achieve higher filtering performance, this conventional *E*-plane waveguide BPF needs to cascade more resonance cavities with the form of high order, which will result in a larger size.

Recently, some compact *E*-plane waveguide filters were presented using several metal strips on the inserted substrate [16]–[18]. For instance, in [16], a *Ka*-band *E*-plane waveguide filter using multiple folded half-wavelength strip resonators was proposed. Nevertheless, this method will be hardly used for the design of *W*-band waveguide filters, since the physical length of the resonator will be shorter at *W*-band frequencies so that the strip resonator cannot be easily folded from the perspective of manufacturing limitation. Therefore, the resonator with longer physical length will be a good candidate for the design of waveguide filter working at *W*-band or even higher frequencies, which has more degree of freedom compared with the half-wavelength strip resonator.

In this letter, a *W*-band *E*-plane waveguide BPF using two metal strips and a meander ring resonator (MRR) is presented, in which one transmission zero (TZ) is located at the lower stopband and the other two TZs at the upper stopband. The center frequency, fractional bandwidth (FBW), and skirt selectivity of the proposed waveguide BPF can be easily manipulated by tuning the structural parameters. Finally, a fabricated sample is measured, which agrees well with the expected simulation results.

II. Design of the E-Plane Waveguide BPF

An MRR is designed on an FSD220G substrate (thickness $h = 0.127$ mm, relative permittivity $\varepsilon_r = 2.2$, and loss tangent $\delta = 0.0009$) and then the substrate is embedded into the central *E*-plane of a WR-10 standard waveguide, as shown in Fig. 1. A tunable TZ can be obtained to achieve high selectivity for the design of *W*-band *E*-plane waveguide BPF. As the parameter g increases and the other parameters are fixed, the position of the TZ will be moved left gradually.

Manuscript received July 6, 2021; accepted August 6, 2021. Date of publication August 9, 2021; date of current version December 6, 2021. This work was supported in part by the FY2019 JSPS Postdoctoral Fellowship for Research in Japan under Grant P19350, in part by the Natural Science Foundation of Shaanxi Province under Grant 2021JQ-060, and in part by the "Siyuan Scholar" Fellowship of XJTU. *(Corresponding author: Kai-Da Xu.)*

Kai-Da Xu is with the School of Information and Communications Engineering, Xi'an Jiaotong University, Xi'an 710049, China, and also with the Department of Communications Engineering, Tohoku University, Sendai 980-8579, Japan (e-mail: kaidaxu@ieee.org).

Shengpei Xia and Anxue Zhang are with the School of Information and Communications Engineering, Xi'an Jiaotong University, Xi'an 710049, China.

Ying-Jiang Guo is with the Microsystem and Terahertz Research Center, China Academy of Engineering Physics, Chengdu 610200, China.

Jianlei Cui is with the State Key Laboratory for Manufacturing Systems Engineering, Xi'an Jiaotong University, Xi'an 710049, China.

Qiang Chen is with the Department of Communications Engineering, Tohoku University, Sendai 980-8579, Japan.

Color versions of one or more figures in this letter are available at https://doi.org/10.1109/LMWC.2021.3103638.

Digital Object Identifier 10.1109/LMWC.2021.3103638

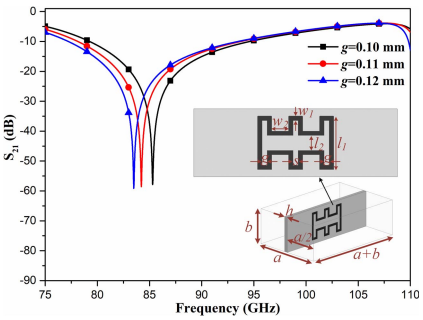

Fig. 1. Simulated results of a WR-10 standard waveguide with an MRR in the center, where $a = 2.54$ mm, $b = 1.27$ mm, $h = 0.127$ mm, $l_1 = 1$ mm, $l_2 = 0.28$ mm, $w_1 = 0.08$ mm, $w_2 = 0.32$ mm, and $s = 0.1$ mm.

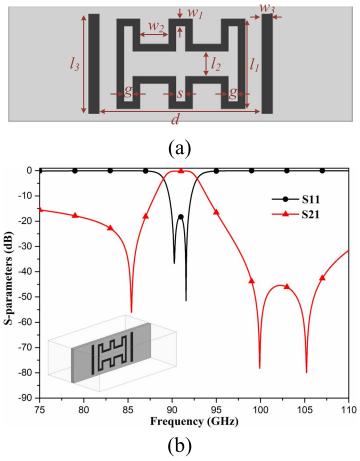

Fig. 2. (a) Detailed layout of the metal layer on the substrate with the parameters set as follows (unit: mm): $l_1 = 1$, $l_2 = 0.28$, $l_3 = 1.1$, $w_1 = 0.08$, $w_2 = 0.32$, $w_3 = 0.12$, $g = 0.1$, $s = 0.1$, $d = 1.8$. (b) S-parameter simulated results of the proposed BPF.

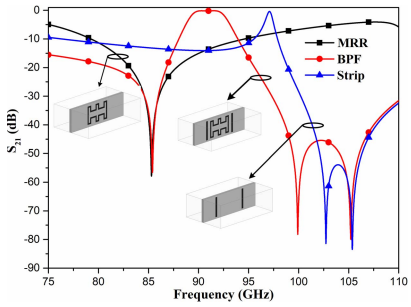

Fig. 3. Simulated performance comparisons among the structures with only two metal strips, with only MRR, and the designed BPF.

In order to realize a bandpass filtering response, two metal strips are loaded on both sides of the MRR, as seen in Fig. 2(a). Consequently, a high-selectivity BPF is constructed with three TZs at the out-of-band, whose simulated frequency response is illustrated in Fig. 2(b). Two resonances are generated by the two-strip structure, which can be used as the TZs at the upper stopband of the proposed BPF. To further study the operating mechanism of the BPF, Fig. 3 demonstrates the simulated performance comparisons among the structures with only two metal strips, with only MRR, and the designed BPF. As can be seen, the TZ at the lower stopband is only determined by the MRR and its position remains unchanged at 85.4 GHz even though the two metal strips are added. At the upper stopband,

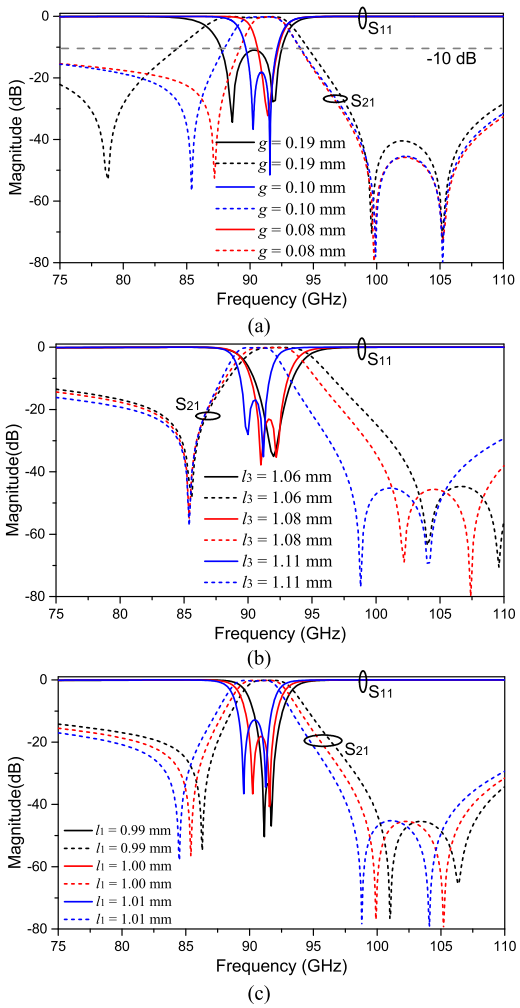

Fig. 4. Simulated S-parameters with different values of (a) g, (b) l_3, and (c) l_1.

the two TZs are yielded from the two metal strips. Due to the insertion of MRR in the middle of the two metal strips, the coupling between the two metal strips will be changed. Therefore, the distance between the two TZs caused by the coupling will be changed accordingly.

The TZ at the lower stopband and the other two TZs at the upper stopband can be independently controlled by the parameters of the MRR and strips, respectively (i.e., g and l_3). As shown in Fig. 4(a), when the value of g decreases from 0.19 to 0.08 mm, the first TZ at the left edge of the passband will be adjusted from 78.8 to 87.2 GHz while the other two TZs keep fixed. The maximum FBW will be 7.8% when g increases to 0.19 mm under the return loss (RL) condition of over 10 dB within the passband. In contrast, as seen in Fig. 4(b), the two TZs at the right edge of the passband can be also tuned as the value of l_3 changes while the first TZ remains fixed. Thus, the FBW and frequency selectivity of the BPF can be easily manipulated by tuning the values of g and l_3. Moreover, the parameter l_1 can adjust the center frequency of the designed BPF as illustrated in Fig. 4(c).

To understand the principle behind the presented filter, a simplified *LC* equivalent circuit is given in Fig. 5(a). The two metal strips can be approximately represented by two same series *LC* resonators $R1$ which are made up of L_1 and C_1.

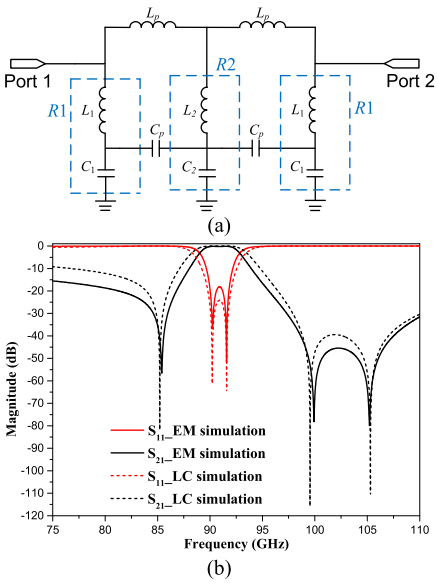

Fig. 5. (a) Simplified *LC* equivalent circuit model of the designed BPF. (b) Comparisons between the EM simulation and *LC* circuit model analysis.

On the other hand, the MRR is equivalent to a series *LC* resonator *R*2 expressed by L_2 and C_2. The capacitive coupling and inductive coupling between the MRR and metal strips are equivalently demonstrated by two same capacitors (i.e., C_p) and two identical inductors (i.e., L_p), respectively. The case of the designed BPF with parameters in the caption of Fig. 2 is analyzed using the proposed *LC* equivalent circuit model. The generation of the TZs and transmission poles (TPs) can be explained by the mechanism of the *LC* resonator pair with proximity coupling [19]. As shown in Fig. 5(b), the simulated S-parameters of the *LC* equivalent circuit agree reasonably well with those of the electromagnetic (EM) simulations, both of which have two resonance frequencies and three TZs. The values of these capacitors and inductors shown in Fig. 5(a) are as follows: $C_1 = 0.0204$ pF, $C_2 = 0.0741$ pF, $C_p = 0.0015$ pF, $L_1 = 0.1137$ nH, $L_2 = 0.0424$ nH, and $L_p = 0.0204$ nH.

III. Fabrication and Measurement

To validate the proposed idea and show the performance of the designed waveguide BPF, a prototype example is manufactured by milling machine using two aluminum split blocks with gold coating for antioxidation, as shown in Fig. 6. The inserted substrate illustrated in Fig. 6 is fabricated using the commercially available printed circuit board technology. The filter measurement is carried out by an Agilent N5247A network analyzer with 75–110 GHz frequency extenders.

Fig. 7 shows the EM simulation and measurement results of *S*-parameters of the proposed filter, which are reasonably in good agreement. The slight discrepancy between simulations and measurements may be caused by the inaccuracy of the loss tangent or the unperfected combination of the waveguide and the substrate. The BPF has achieved a measured 3-dB bandwidth from 88.9 to 93.7 GHz with a center frequency of 91.3 GHz. Within the passband, the measured minimum IL is 1.6 dB including the loss of 9.2 mm WR-10 feeding waveguide. The RL at the center frequency is 18 dB. Table I tabulates the characteristic comparisons of the proposed *W*-band BPF with some previously reported works. It can be seen that our work at *W*-band has compact size, low IL, and good frequency selectivity with multiple TZs.

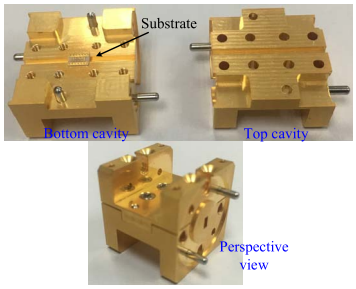

Fig. 6. Fabricated photograph of the presented waveguide BPF.

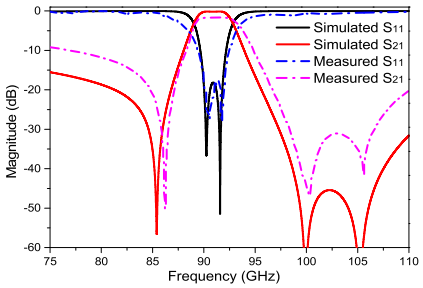

Fig. 7. EM simulation and measurement results of the waveguide BPF.

TABLE I
Comparisons With Some Previous *W*-Band BPFs

	CF# (GHz)	Nos. of TZs & TPs	FBW (%)	IL (dB)	RL (dB)	Size (mm^3)	ξ_{ROR}* (L & U) (dB/GHz)	Technology
[2]	88.34	0 & 5	12.1	1.94	>18	7.94×2.54×1.27	10.2 & 3.3	Micro laser sintering process
[9]	93	2 & 3	3.4	4.3	>13.5	4.2×2.2×0.07	13.6 & 13.6	GaAs on-chip process
[20]	88.47	0 & 4	9.7	1.1	>15	12.3×2.54×1.27	4.5 & 5.3	SU-8 process
This work	**91.3**	**3 & 2**	**5.3**	**1.6**	**>18**	**3.81×2.54×1.27**	**9.5 & 5.9**	**Conventional milling machine process**

#CF: center frequency. *Transition band roll-off rates $\xi_{ROR}=|\delta_{-20dB}-\delta_{-3dB}|/|f_{-20dB}-f_{-3dB}|$, where $\delta_{-20/-3dB}$ denotes the 20/3dB attenuation point, and $f_{-20/-3dB}$ is the 20/3dB stopband frequency of $|S_{21}|$. L and U denote lower and upper transition band roll-off rates, respectively.

IV. Conclusion

A compact *W*-Band *E*-Plane waveguide BPF with three TZs has been designed and measured. The TZ at the lower stopband and the other two TZs at the upper stopband can be independently controlled by the parameters of the MRR and strips, respectively. The EM simulated and measured results of the fabricated waveguide BPF example are in reasonably good agreement. Due to its simple topology with multiple TZs, low in-band IL, and ease of extending to the higher order filter design, the proposed BPF will be a good candidate for the practical applications in millimeter-wave circuits and systems.

REFERENCES

[1] C. A. Leal-Sevillano, J. R. Montejo-Garai, M. Ke, M. J. Lancaster, J. A. Ruiz-Cruz, and J. M. Rebollar, "A pseudo-elliptical response filter at W-band fabricated with thick SU-8 photo-resist technology," *IEEE Microw. Wireless Compon. Lett.*, vol. 22, no. 3, pp. 105–107, Mar. 2012.

[2] M. Salek *et al.*, "W-band waveguide bandpass filters fabricated by micro laser sintering," *IEEE Trans. Circuits Syst. II, Exp. Briefs*, vol. 66, no. 1, pp. 61–65, Jan. 2019.

[3] A. Vosoogh, A. A. Brazález, and P.-S. Kildal, "A V-band inverted microstrip gap waveguide end-coupled bandpass filter," *IEEE Microw. Wireless Compon. Lett.*, vol. 26, no. 4, pp. 261–263, Apr. 2016.

[4] Z.-C. Hao, W.-Q. Ding, and W. Hong, "Developing low-cost W-band SIW bandpass filters using the commercially available printed-circuit-board technology," *IEEE Trans. Microw. Theory Techn.*, vol. 64, no. 6, pp. 1775–1786, Jun. 2016.

[5] S. W. Wong, K. Wang, Z.-N. Chen, and Q.-X. Chu, "Design of millimeter-wave bandpass filter using electric coupling of substrate integrated waveguide (SIW)," *IEEE Microw. Wireless Compon. Lett.*, vol. 24, no. 1, pp. 26–28, Jan. 2014.

[6] J. A. Martinez, J. J. de Dios, A. Belenguer, H. Esteban, and V. E. Boria, "Integration of a very high quality factor filter in empty substrate-integrated waveguide at Q-band," *IEEE Microw. Wireless Compon. Lett.*, vol. 28, no. 6, pp. 503–505, May 2018.

[7] Y. Li, L.-A. Yang, L. Du, K. Zhang, and Y. Hao, "Design of millimeter-wave resonant cavity and filter using 3-D substrate-integrated circular waveguide," *IEEE Microw. Wireless Compon. Lett.*, vol. 27, no. 8, pp. 706–708, Aug. 2017.

[8] X. Liu, Z. Zhu, Y. Liu, Q. Lu, X. Yin, and Y. Yang, "Wideband substrate integrated waveguide bandpass filter based on 3-D ICs," *IEEE Trans. Compon., Packag., Manuf. Technol.*, vol. 9, no. 4, pp. 728–735, Apr. 2019.

[9] Y. Xiao, P. Shan, Y. Zhao, H. Sun, and F. Yang, "Design of a W-band GaAs-based SIW chip filter using higher order mode resonances," *IEEE Microw. Wireless Compon. Lett.*, vol. 29, no. 2, pp. 104–106, Feb. 2019.

[10] Y.-J. Guo, K.-D. Xu, X. Deng, X. Cheng, and Q. Chen, "Millimeter-wave on-chip bandpass filter based on spoof surface plasmon polaritons," *IEEE Electron Device Lett.*, vol. 41, no. 8, pp. 1165–1168, Aug. 2020.

[11] K. Ma, S. Mou, and K. S. Yeo, "Miniaturized 60-GHz on-chip multimode quasi-elliptical bandpass filter," *IEEE Electron. Devices Lett*, vol. 34, no. 8, pp. 945–947, Aug. 2013.

[12] K.-D. Xu, X. Zhu, Y. Yang, and Q. Chen, "A broadband on-chip bandpass filter using shunt dual-layer meander-line resonators," *IEEE Electron Device Lett.*, vol. 41, no. 11, pp. 1617–1620, Nov. 2020.

[13] J.-Q. Ding, S.-C. Shi, K. Zhou, D. Liu, and W. Wu, "Analysis of 220-GHz low-loss quasi-elliptic waveguide bandpass filter," *IEEE Microw. Wireless Compon. Lett.*, vol. 27, no. 7, pp. 648–650, Jul. 2017.

[14] K. Zhou, J.-Q. Ding, C.-X. Zhou, and W. Wu, "W-band dual-band quasi-elliptical waveguide filter with flexibly allocated frequency and bandwidth ratios," *IEEE Microw. Wireless Compon. Lett.*, vol. 28, no. 3, pp. 206–208, Feb. 2018.

[15] Y. Konishi and K. Uenakada, "The design of a bandpass filter with inductive strip—Planar circuit mounted in waveguide," *IEEE Trans. Microw. Theory Techn.*, vol. MTT-22, no. 10, pp. 869–873, Oct. 1974.

[16] J. Y. Jin, X. Q. Lin, Y. Jiang, and Q. Xue, "A novel compact E-plane waveguide filter with multiple transmission zeroes," *IEEE Trans. Microw. Theory Techn.*, vol. 63, no. 10, pp. 3374–3380, Oct. 2015.

[17] X. Q. Lin, J. Y. Jin, Y. Jiang, and Y. Fan, "Metamaterial-inspired waveguide filters with compact size and sharp skirt selectivity," *J. Electromagn. Waves Appl.*, vol. 27, no. 2, pp. 224–232, Sep. 2013.

[18] M. Mrvić, M. Potrebić, and D. Tošić, "Compact E plane waveguide filter with multiple stopbands," *Radio Sci.*, vol. 51, no. 12, pp. 1895–1904, Dec. 2016.

[19] Q. Xue and J. Y. Jin, "Bandpass filters designed by transmission zero resonator pairs with proximity coupling," *IEEE Trans. Microw. Theory Techn.*, vol. 65, no. 11, pp. 4103–4110, Nov. 2017.

[20] X. Shang, M. Ke, Y. Wang, and M. Lancaster, "Micromachined W-band waveguide and filter with two embedded H-plane bends," *IET Microw., Antennas Propag.*, vol. 5, no. 3, pp. 334–339, Feb. 2011.